ELSEVIER

Biophysical Chemistry 114 (2005) 1–12

Biophysical Chemistry

http://www.elsevier.com/locate/biophyschem

Thermal denaturation of the BRCT tandem repeat region of human tumour suppressor gene product BRCA1

Serapion Pyrpassopoulos[a], Angela Ladopoulou[a], Metaxia Vlassi[a], Yannis Papanikolau[b], Constantinos E. Vorgias[c], Drakoulis Yannoukakos[a,*], George Nounesis[a]

[a]*National Centre for Scientific Research "Demokritos", Patriarchou Gregoriou St., 153 10 Aghia Paraskevi, Greece*
[b]*Institute of Molecular Biology and Biotechnology, Foundation for Research and Technology, 711 10 Heraklion, Greece*
[c]*Department of Biology, National and Kapodistrian University of Athens, 157 84 Zografou, Greece*

Received 29 July 2004; received in revised form 14 September 2004; accepted 30 September 2004
Available online 5 November 2004

Abstract

Reduced stability of the tandem BRCT domains of human *BReast CAncer 1* (*BRCA1*) due to missense mutations may be critical for loss of function in DNA repair and damage-induced checkpoint control. In the present thermal denaturation study of the BRCA1 BRCT region, high-precision differential scanning calorimetry (DSC) and circular dichroism (CD) spectroscopy provide evidence for the existence of a denatured state that is structurally very similar to the native. Consistency between theoretical structure-based estimates of the enthalpy (ΔH) and heat capacity change (ΔC_p) and the calorimetric results is obtained when considering partial thermal unfolding contained in the region of the conserved hydrophobic pocket formed at the interface of the two BRCT repeats. The structural integrity of this region has been shown to be crucial for the interaction of BRCA1 with phosphorylated peptides. In addition, cancer-causing missense mutations located at the inter-BRCT-repeat interface have been linked to the destabilization of the tandem BRCT structure.

Keywords: BRCT; BRCA1; Breast cancer

1. Introduction

Loss-of-function germ line mutations in the 1863-residue *BReast CAncer 1* (*BRCA1*) gene product predispose carriers to breast/ovarian cancer [1,2]. Most frequently, they are frame shifts or nonsense mutations leading to truncated proteins. However, a large number of missense mutations have been identified and although their functional role in carcinogenesis remains to be determined, a handful have already been linked to the pathological phenotype. Up to recently, several missense mutations at the C-terminal BRCT (BRCA1 C-Terminal) repeat region of BRCA1 have been associated to cancer. On the other hand, over 100 missense mutations have been deposited at the Breast Cancer Information Core (BIC) as unclassified variants, although functional studies have shown that several lead to loss of function in vitro [3–5].

The ubiquitously expressed BRCA1 protein is implicated in DNA repair and recombination, checkpoint control of cell cycle, and transcription [6,7]. Most of these functions require the integrity of a tandem repeat of the conserved BRCT domain (BRCT-tan). BRCT repeats consist of 95–100 residues. They are encountered in a multitude of proteins of different apparent functions as single, tandem, or multiple (as many as eight repeats) [8]. Despite the various functional differences, DNA damage response appears to be common theme for all the BRCT-containing proteins. BRCT repeats are expected to interact in forming complexes with non-BRCT proteins [9] and DNA [10].

The crystal structures of the single BRCT repeat from the XRCC1 protein [11] and ligase III [12], BRCT-tan from

* Corresponding author. Tel.: +30 210 6503936; fax: +30 210 6543526.
E-mail address: yannouka@rrp.demokritos.gr (D. Yannoukakos).

0301-4622/$ - see front matter © 2004 Elsevier B.V. All rights reserved.
doi:10.1016/j.bpc.2004.09.014

human BRCA1 [13], and BRCT-tan from human 53BP1 [14,15] follow a highly conserved structural motif. It consists of a parallel four-stranded β-sheet located at the central part of the fold surrounded by three α-helices. Two of them (α1, α3) are solidly packed against one side of the β-sheet, while the third (α2) is packed against the opposite side. Specifically, for BRCT-tan, the interaction of the α2 helix of the N-terminal repeat with the helices α1 and α3 of the C-terminal repeat gives rise to the formation of a conserved, almost all-hydrophobic interrepeat interface characterized by tight knobs-in-holes-type packing. A flexible BRCT-repeat-interconnecting 23-residue linker is also involved in the interface formation, because the α-helix at its center packs right against the inter-BRCT interface.

It has recently been shown that only BRCT-tan and not single BRCT repeats interact with phosphorylated proteins [16–18]. In human cells, BRCA1 interacts with phosphorylated BACH1 helicase to activate cell cycle checkpoint in response to DNA damage. For this interaction, the motif pSer-*X*-*X*-Phe (where *X* could be any amino acid) of BACH1 binds with high affinity to BRCT-tan [16–18]. Recent crystallographic studies of the complex of BRCT-tan with optimized phosphorylated peptides have demonstrated that phosphoserine binds through a hydrogen bond network into a conserved shallow pocket at the N-terminal BRCT repeat. Phenylalanine, on the other hand, is recognized by the hydrophobic inter-BRCT-interface interacting primarily through van der Waals contacts with the C-terminal BRCT repeat. This "two-knobs" binding model requires the structural integrity of both binding sites for high-affinity binding [19–21]. Cancer-causing missense mutations located at the inter-BRCT-repeat interface can destabilize the structure [13]. Previous chemical denaturation experiments of BRCT-tan of human BRCA1 have shown that the overall free energy of unfolding is high (ΔG=14.2 kcal/mol); most importantly, that the unfolding occurs via an aggregation-prone partly folded intermediate [22]. Missense mutations were shown to cause a reduction in the thermodynamic stability of the native relative to the intermediate [22]. Loss of function occurring in disease-associated mutants has been linked to a decrease of the thermodynamic stability relative to the wild-type [23,24]. In this context, biophysical investigations of the unfolding mechanism of BRCT-tan are expected to provide important information pertaining to the molecule's stability.

For this study, we have cloned and overproduced the tandem BRCT repeat region (a.a. 1646–1859) of human BRCA1 in a highly soluble and stable form. We have studied the heat denaturation of the polypeptide via high-sensitivity differential scanning calorimetry (DSC) and circular dichroism (CD). We show that heat denaturation of BRCT-tan involves a denatured state that is only partly unfolded. Finally, we use theoretical structure-based thermodynamic analysis to explore the role of the hydrophobic inter-BRCT interface region in the observed partial unfolding.

2. Materials and methods

2.1. Gene subcloning

For overproducing the BRCT domain, we used the exact same cDNA length described by Williams et al. [13]. The encoding region for human BRCA1 BRCT-tan domain (a.a 1646–1859) was amplified by PCR from a plasmid kindly provided by Prof. A.N. Monteiro (Cornell University), using the following primers: (i) BRCT (*Nde*I), aca tat ggt caa caa aag aat gtg cat ggt g, and (ii) BRCT (*Bam*HI), agg atc ctc agg gga tct ggg gta tca gg, with *Nde*I and *Bam*HI restriction sites at their 5′ and 3′ ends, respectively. The resulting 750 bp PCR product was ligated into pCR2.1 cloning vector and transformed into *E. coli* INVaF' according to the manufacturer's instructions (Invitrogen). It was then sequenced using the ABI310 sequencer (Applied Biosystems). Plasmid isolated from a positive clone was submitted to digestion with *Nde*I and *Bam*HI, and the insert was cloned into pET-3a expression vector (Novagen) and transformed into Novablue competent cells. Plasmid DNA isolated from the positive clones was then transformed into *E. coli* BLR(DE3)pLysS expression strain (Novagen).

2.2. Protein expression and purification

The BRCT-tan domain was overproduced in *E. coli* BLR(DE3)pLysS strain and purified using a combination of SP-Sepharose Fast Flow column (Pharmacia) and a Q-Sepharose High Performance column (Pharmacia). Protein concentration was measured spectrophotometrically using an extinction coefficient of 1.475 for 1 mg/ml at 280 nm [25]. SDS-PAGE analysis was carried out according to Laemmli [26].

2.3. Gel filtration chromatography

Gel filtration chromatography experiments were carried out on a Superose™ 12 prepacked HR10/30 column (Amersham Biosciences). The column was run with an FPLC® system at a flow rate of 0.4 ml/min. The sample volume loaded each time was 0.2 ml. The absorption A of the eluent was monitored at 280 nm.

2.4. Circular dichroism spectroscopy (CD)

CD measurements were conducted using a JASCO-715 spectropolarimeter with a Peltier type cell holder, which allows for temperature control. Wavelength scans in the far (190 to 260 nm) and the near (260 to 360 nm) UV regions were performed in Quartz SUPRASIL (HELLMA) precision cells of 0.1 and 1 cm path length, respectively. Each spectrum was obtained by averaging five to eight successive accumulations with a wavelength step of 0.2 nm at a rate of 20 nm min^{-1}, response time 1 s, and band width 1 nm.

Buffer spectra were accumulated and subtracted from the sample scans. The absorption spectra were recorded selecting the UV (single) mode of the instrument. CD experiments involving thermal scanning have been carried out in the range from 20 to 90 °C, at 213.5, 222, and 225 nm, and heating scan rates ranging from 0.3 to 2.5 K/min.

2.5. Differential scanning calorimetry (DSC)

For the high-sensitivity calorimetric measurements, the VP DSC calorimeter was employed (Microcal, Northampton, USA) [27]. Protein concentrations used in the DSC studies varied between 0.3 and 2.0 mg/ml. Protein samples and buffer reference solutions were properly degassed and carefully loaded into the cells to avoid bubble formation. Four to five reference scans with buffer-filled cells (sample and reference cell volume is 0.523 ml) preceded each sample run to achieve near perfect baseline repeatability. A typical DSC experiment consisted of a heating scan at a programmed heating rate followed by a second heating scan, which probed the irreversibility of the transitions under study. Experiments characterized by large-scale aggregation and precipitation effects are carried out with the DSC unit operating sideways to minimize precipitation-induced calorimetric artefacts, as recommended by the manufacturer. Whenever needed, the difference in the heat capacity between the initial and final states was modelled by a sigmoidal chemical baseline [28] using the ORIGIN DSC software. Baseline subtraction and analysis of the calorimetric data were carried out via nonlinear least squares fitting procedures of the ORIGIN 5.0 software.

2.6. Structure-based thermodynamic analysis

The structure-based parametric analysis proposed by Gomez et al. [29] has been employed for estimating the heat capacity difference between the pre- and postthermal denaturation baselines (ΔC_p), and by Hilser et al. [30] for estimating the change in the total enthalpy (ΔH_{cal}). The analysis is described by the following set of equations:

$$\Delta C_p = \Delta C_{p,c} + \Delta C_{p,b} \tag{1a}$$

Where $\Delta C_{p,c}$ is the hydration contribution,

$$\Delta C_{p,c} = a(T)\Delta \mathrm{ASA}_{ap} + b(T)\Delta \mathrm{ASA}_{\mathrm{pol}} \tag{1b}$$

and $\Delta C_{p,b}$ is the contribution of noncovalent interactions within the protein molecule,

$$\Delta C_{p,b} = [p + q(T - 25)]\Delta \mathrm{ASA}_{\mathrm{Total}} \tag{1c}$$

In the above equations, $\Delta \mathrm{ASA}_{ap}$ is the change, after denaturation, in the solvent accessible apolar surface area and correspondingly $\Delta \mathrm{ASA}_{\mathrm{pol}}$ of the polar surface area, $a(T)$=0.45+2.63 10^{-4} (T−25)−4.2 10^{-5} (T−25)^2 in units of cal/(K mol Å^2) and $b(T)$=−0.265+2.85 10^{-4} (T−25)+4.31 10^{-5} (T−25)^2 in units of cal/(K mol Å^2), p and q are global fitting parameters for C_p: p=8.7×10^{-3} cal/(K mol Å^2) and q=6.43×10^{-4} cal/(K^2 mol Å^2).

The corresponding structure-based parametric equation for ΔH_{cal} is as follows:

$$\Delta H_{\mathrm{cal}} = \left(a_{ap} + b_{ap}U_{ap}^6\right)\Delta \mathrm{ASA}_{ap} + \left(a_{\mathrm{pol}} + b_{\mathrm{pol}}U_{\mathrm{pol}}^6\right)\Delta \mathrm{ASA}_{\mathrm{pol}} + b_{\mathrm{mix}}U_{\mathrm{mix}}^6\Delta \mathrm{ASA}_{\mathrm{Total}} \tag{2}$$

Here, U is effectively a Lennard–Jones packing parameter for the polar, apolar, and mixed (polar–apolar) interactions within the protein molecule. The following values for the parameters (a) and (b) have been used: a_{ap}=−12.96, b_{ap}=25.34, a_{pol}=24.38, b_{pol}=16.57, b_{mix}=16.42. The values of U_{ap}, U_{pol}, and U_{mix} have all been assumed equal and dependent only upon the packing density. For the calculations, the value U=0.85 is used. It was derived by Hilser et al. [30] as an average upper boundary for the packing parameter. Calculations of accessible surface areas (ASAs) have been carried out using the DSSP program [31].

3. Results

The construct used to express BRCT-tan (residues 1646–1859) was created by considering the limited proteolysis experiments described by Williams et al. [13]. No tag was introduced to the produced protein, which was more than 99% pure, highly soluble, and stable for several months at 4 °C. SDS-PAGE showed the presence of a single band at the expected MW (~25 kDa). Far-UV CD spectroscopy at 25 °C, pH 7.0, 10 mM Na phosphate revealed a folded polypeptide (Fig. 1). Analysis of the spectrum via CONTIN [32], K2D [33], SELCON [34], and CDNN [35,36] algorithms and averaging of the results leads to the following estimates for the secondary structure elements: α-helix=33.0±2.7%, β-sheet=19.8±1.9%, and remainder 47.2±4.5%. These results are in excellent agreement with the crystal structure of BRCT-tan (RCSB entry: 1JNX) [13]. Variation of pH, between pH 6.0 and pH 9.0, does not induce changes in the secondary structure. Identical far-UV CD spectra have been obtained at 25 °C (Fig. 1) for pH 8.5, 10 mM Tris–HCl, 500 mM NaCl, a pH value used for spectroscopic measurements in chemical denaturation studies [22]; pH 6.0, 5 mM Na phosphate, 125 mM NaCl, just above the theoretically expected isoelectric point; pH 9.0, 10 mM Tris–HCl, extensively used in the present calorimetric study.

3.1. Calorimetry

The heat denaturation of BRCT-tan has been studied by high-sensitivity DSC at pH 7.0 and pH 9.0 for various protein concentrations (C_t). Additional calorimetric experiments at pH 6.0 produced poor quality data that were

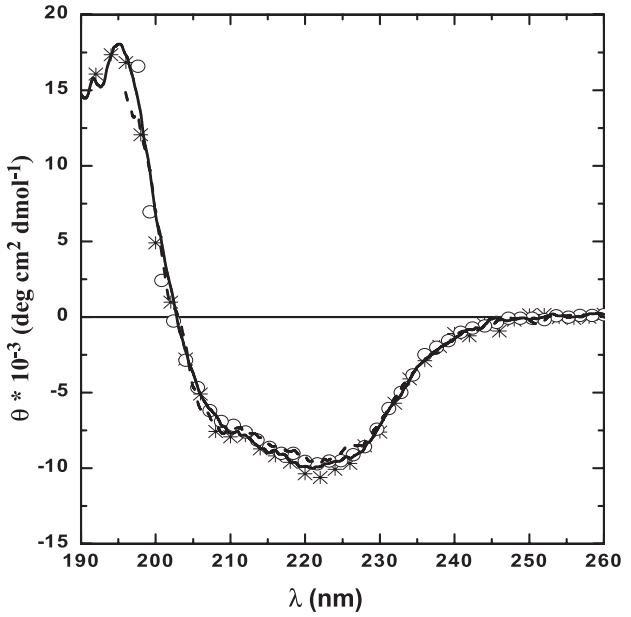

Fig. 1. Identical far-UV CD normalized spectra for native BRCT-tan at 25 °C for various pH conditions and buffers: pH 6.0, 5 mM Na-phosphate, 125 mM NaCl (asterisks); pH 7.0, 10 mM Na phosphate (dashed line); pH 8.5, 10 mM Tris–HCl, 500 mM NaCl (open circles); pH 9.0, 10 mM Tris–HCl (solid line).

gravely affected by aggregation and precipitation in the denatured state. The DSC traces at pH 7.0 10 mM Na phosphate buffer are presented in Fig. 2. The heat denaturation profile, heat capacity change at constant pressure vs. temperature (<ΔC_p> vs. T), shows an endothermic irreversible transition at T_m (temperature at maximum <ΔC_p>)=50.3 °C. For all concentrations, the high-T side of the <ΔC_p> peak overlaps with a second DSC anomaly, which can most likely be attributed to further unfolding, aggregation, and precipitation of the denatured molecules. The formation of precipitated aggregates of denatured BRCT-tan is visible at $T>T_m$. The kinetically controlled thermal reaction is dependent upon the DSC heating scan rate (u) but is independent of C_t as expected for the unfolding (first-order reaction) of a monomeric protein. The aggregation-induced distortion of the <ΔC_p> peaks, as well as of the baseline in the denatured state renders any attempt for analysis very difficult. Nevertheless, rough estimates of calorimetric and activation parameters for the kinetically controlled unfolding were derived using fits of a two-state irreversible model [37] [$N \rightarrow I$, where (N) is the native and (I) is the irreversibly denatured state] leading to the following values for the thermodynamic parameters: total enthalpy change ΔH_{cal}=51.2±6.1 kcal/mol and activation energy E_α=121.0±16.8 kcal/mol.

The corresponding DSC curves at pH 9.0, 10 mM Tris–HCl reveal a situation analogous to pH 7.0 yet more promising for obtaining more reliable calorimetric results. The profiles of <ΔC_p> vs. T exhibit an irreversible endothermic peak, only this time, the low-C_t samples appear to be free of aggregation-related distortions. The transition occurs at T_m ~47 °C, while the thermal anomaly associated with aggregation and precipitation occurs even at 50 °C higher T (for C_t <0.5 mg/ml), allowing for an accurate determination of the baseline in the denatured state (Fig. 3). As expected for the kinetically controlled peak, the values of T_m exhibit a pronounced nonlinear u dependence.

Interestingly, the <ΔC_p> peaks, as illustrated in Fig. 4, are dependent upon C_t in a manner (T_m increasing with increasing C_t) shown to describe the unfolding of a native oligomer also involving dissociation into denatured monomers [37,38]. The thermal behavior prompted the investigation of the oligomerization properties of native BRCT-tan at low-salt pH 9.0 solutions by gel filtration chromatography. The results point straightforwardly to a dimeric native state (Fig. 5). In 10 mM Na phosphate buffer pH 7.0, native BRCT-tan elutes with a sharp peak corresponding to the monomer MW and a very minor peak (<1%) corresponding to the dimer. The elution profile is entirely reversed at pH 9.0 10 mM Tris–HCl. It exhibits a sharp dominant peak (>99%) corresponding to the dimer MW, whereas the presence of monomeric BRCT-tan is reduced to less than 1%.

We have attempted to analyze the DSC peak for u=1.5 K/min, for which aggregation-induced distortions appear to be minimal. The model for an irreversible unfolding-coupled-

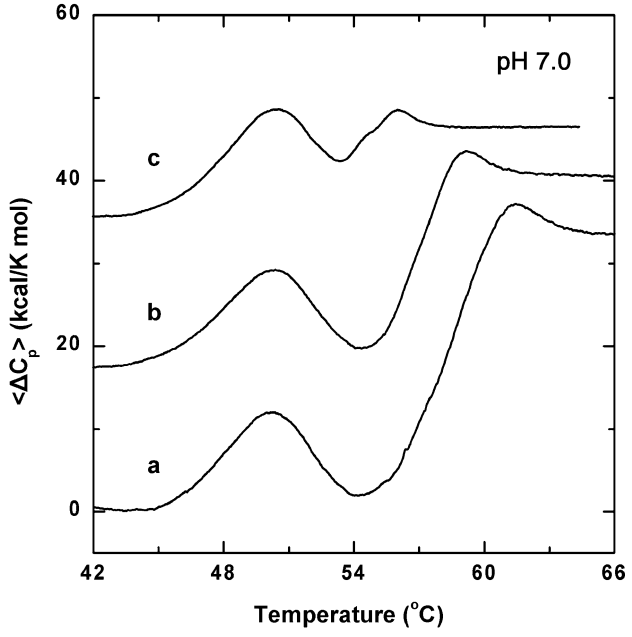

Fig. 2. DSC profiles (<ΔC_p> vs. T) for the thermally induced denaturation of BRCT-tan at pH 7.0 10 mM Na phosphate at various concentrations C_t and heating scan rate u=1 K/min. The three concentrations shown are a=0.36 mg/ml, b=0.5 mg/ml, and c=0.7 mg/ml. The data have been shifted vertically for clarity. The profiles exhibit two endothermic peaks. The higher-T thermal anomaly involves the formation of aggregated precipitates.

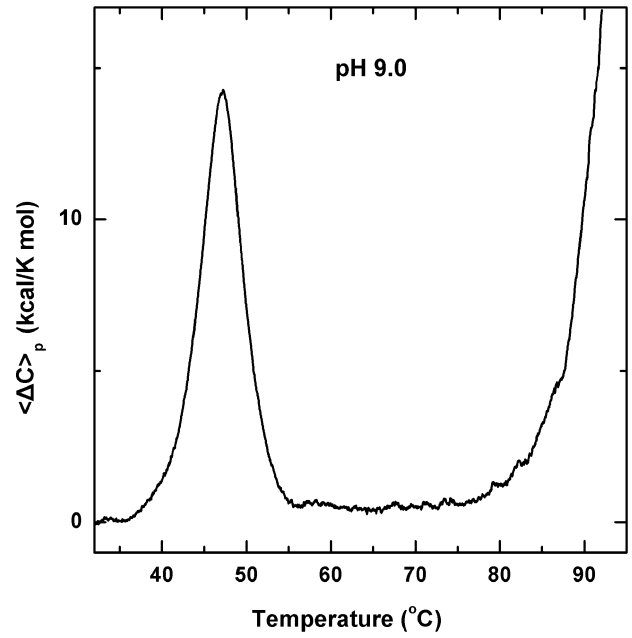

Fig. 3. $<\Delta C_p>$ vs. T trace for the unfolding of BRCT-tan at pH 9.0, 10 mM Tris–HCl, C_t=0.45 mg/ml and u=1.5 K/min. The higher-T transition occurs at ~106 °C, over 50° above T_m minimizing distortions in the denaturation $<\Delta C_p>$ profile due to the overlap between the two DSC peaks.

to-oligomer-dissociation proposed by Sanchez-Ruiz [37] failed to fit the DSC data for any value of the oligomerization index n. The fits were particularly poor at the high-T side of the $<\Delta C_p>$ peak due to the steep and asymmetric shape of the theoretical curves. This is indicative that a Lumry–Eyring model including a reversible followed by a slow irreversible step is more suitable for the description of the denaturing sequence:

$$N_2 \underset{k_{-1}}{\overset{k_1}{\rightleftarrows}} 2D \xrightarrow{k_2} I \tag{3}$$

Here, based on the results from gel filtration, (N_2) is the native dimer, (D) is the reversibly denatured monomer, and (I) is the irreversibly denatured state.

The dependence of the DSC peaks upon u at constant C_t=0.45 mg/ml is displayed in Fig. 6 (calorimetric parameters are included in Table 1). ΔH_{cal} and $T_{1/2}$ (temperature for which half of the native population has been denatured) are plotted as a function of u in Fig. 7. It can readily be observed that ΔH_{cal} is practically constant, independent of u with an average value ΔH_{cal}=91.6±7.3 kcal/mol (Fig. 7, upper panel). On the other hand, $T_{1/2}$ exhibits a pronounced nonlinear u dependence (Fig. 7, lower panel). Because the maximum u attained by our high-sensitivity calorimeter is 1.5 K/min, CD spectroscopy was also employed to probe $T_{1/2}$ behavior at even higher u. The $T_{1/2}$ values are derived by continuously monitoring the changes in the CD spectrum at λ=213.5 and 225 nm, as a function of temperature, for u varying from 0.5 to 2.5 K/min. From the data presented in Fig. 6, it is apparent that at

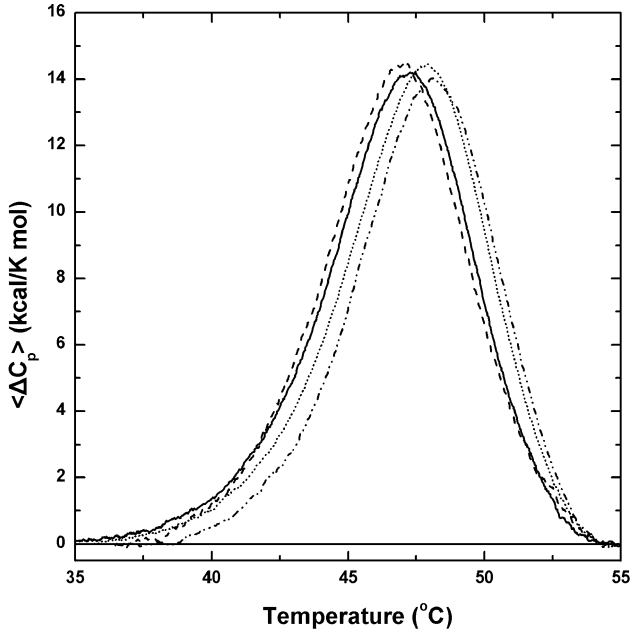

Fig. 4. DSC traces for the unfolding of BRCT-tan at pH 9.0 10 mM Tris–HCl for four different concentrations C_t: 0.3 mg/ml (dash), 0.45 mg/ml (solid), 0.5 mg/ml (short dash), and 0.6 mg/ml (dash dot dot). T_m for the endothermic peak increases with increasing C_t indicating the dissociation of a native oligomer into denatured monomers. Baselines have been subtracted for the traces presented here. The corresponding calorimetric parameters are included in Table 1.

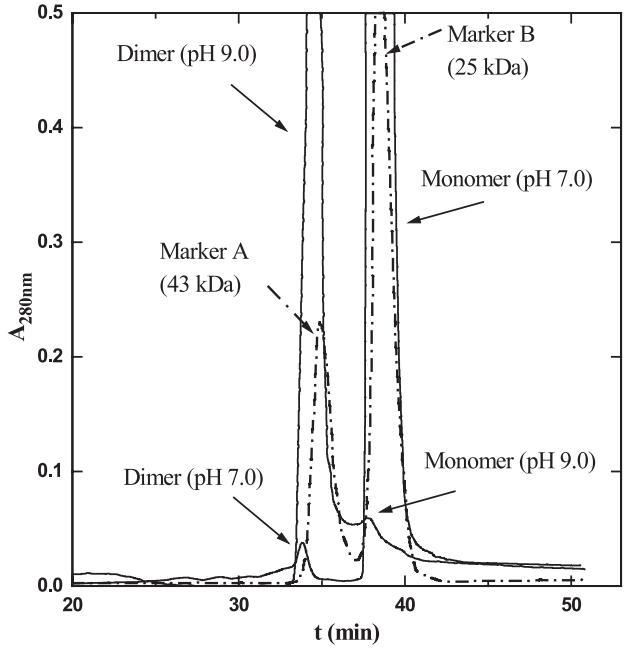

Fig. 5. Gel-filtration experiments on Superose™ 12: BRCT-tan elutes as a sharp peak at a molecular weight corresponding to the monomer (25 kDa) in 10 mM sodium phosphate buffer pH 7.0 and shifts to a molecular weight corresponding to the dimer (50 kDa) in 10 mM Tris–HCl buffer pH 9.0. The dot–dash line monitors the elution profile of two markers. The peak marked as A corresponds to Ovalbumin (43 kDa), and the peak marked as B corresponds to Chymotrypsinogen A (25 kDa). The markers are part of the LMW gel filtration calibration kit by Amersham Biosciences.

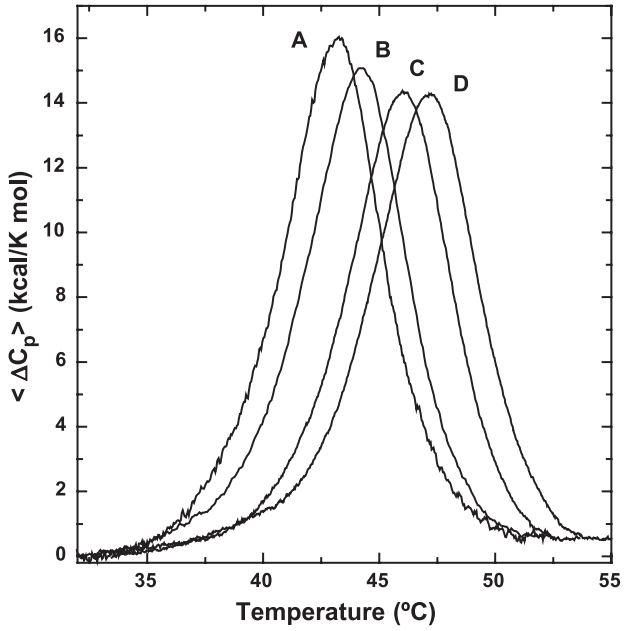

Fig. 6. Experimental DSC curves for the thermal unfolding transition at various scan rates u: (A) u=0.3 K/min; (B) u=0.5 K/min; (C) u=1.0 K/min; and (D) u=1.5 K/min. The calorimetric parameters corresponding to these peaks are included in Table 1.

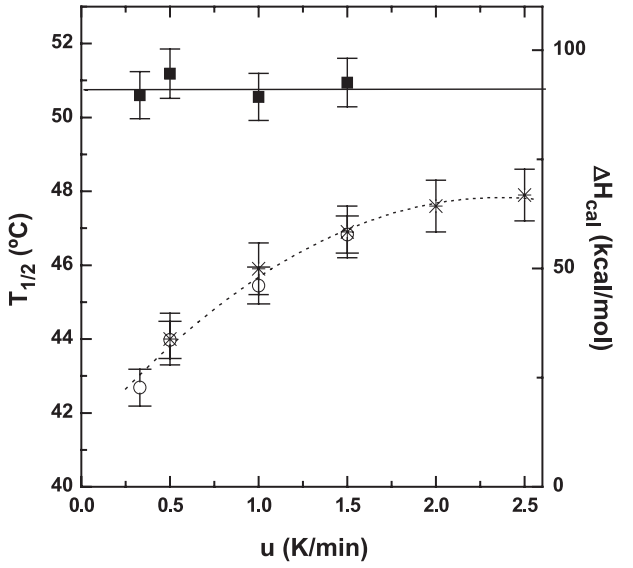

Fig. 7. $T_{1/2}$ (left ordinate, ○ and *) and ΔH_{cal} (right ordinate, ■) are displayed versus the DSC heating scan rate u for constant C_t=0.45 mg/ml. Data for $T_{1/2}$ (i.e., temperature at which half of the unfolding is completed), displayed in the lower panel, have been obtained either by DSC (○) or by CD spectroscopy (*) by heating through the thermal transition at λ=213.5 and 226 nm; the dotted line serves as a guide to the eye. At high u, $T_{1/2}$ reaches an equilibrium plateau value of 47.9 °C. The data for ΔH_{cal} (upper panel) are practically independent of u with an average value of ΔH_{cal}=91.6±7.3 kcal/mol (solid line).

high u, $T_{1/2}$ approaches a plateau value of 47.9 °C. Analogous behavior has been observed for the irreversible unfolding of other proteins [39,40]. It provides evidence that the thermal transition is indeed described by a reversible reaction followed by a relatively slow irreversible step to the final state Eq. (3). At fast heating rates, the effects from kinetic contamination are considerably overcome, and the obtained DSC results are close to the equilibrium values. Moreover, the fact that ΔH_{cal} and ΔC_p are independent of u signifies that the slow irreversible step is athermal, that is, it has minimal contribution to ΔH_{cal} or ΔC_p. Due to the proximity of $T_{1/2}$ at u=1.5 K/min to the equilibrium plateau, the irreversible DSC results, ΔH_{cal} (at u=1.5 K/min)=92.6±5.6 kcal/mol and ΔC_p (at u=1.5 K/min)=0.60±0.08 kcal/K mol directly measured from the DSC traces, may be considered reliable to describe the thermal denaturation of BRCT-tan. Interestingly, the reversible two-state transition model fits the C_t=0.45 mg/ml DSC data leading to ΔH_{cal} estimates that are in good agreement with the experimental results. The corresponding values for the ratio of ΔH_{cal} to the van't Hoff enthalpy change ΔH_{vH} (setting the oligomerization index n=2 for the dissociation of dimer BRCT-tan [41]), increase with u. At u=0.3 K/min $\Delta H_{cal}/\Delta H_{vH}$=0.91 accordingly, at u=0.5 K/min $\Delta H_{cal}/\Delta H_{vH}$=0.99. The ratio reaches the value of 1.02 at u=1.5 K/min.

Table 1
DSC results

u (K/min)	C_t (mg/ml)	$T_{1/2}$ (°C)	ΔH_{cal} (kcal/mol)	ΔC_p (kcal/K mol)
0.3	0.45	42.7±0.6	89.7±5.4	0.52±0.09
0.5	0.45	43.9±0.6	94.7±5.7	0.61±0.09
1.0	0.45	45.7±0.5	89.3±5.4	0.68±0.08
1.5	0.30	46.6±0.5	94.4±5.7	0.63±0.08
1.5	0.45	46.8±0.5	92.6±5.6	0.60±0.08
1.5	0.50	47.5±0.5	97.0±5.8	0.68±0.09
1.5	0.60	47.7±0.5	85.5±5.2	0.71±0.09
1.5	0.70	47.8±0.5	78.1±4.7	0.65±0.09
1.5	0.80	47.9±0.6	76.1±4.6	0.80±0.09

Experimental results for $T_{1/2}$ and ΔH_{cal} and ΔC_p for the thermal unfolding of BRCT-tan at pH 9.0, 10 mM Tris–HCl for various heating DSC scan rates u and BRCT-tan concentration C_t.

The obtained value of ΔC_p=2.80 cal/K mol-residue is small compared to proteins of the same or smaller size than BRCT-tan. In fact, it is one of the smallest reported. For comparison, the corresponding result for the thermal unfolding of the dimeric HIV-1 protease (99 residues in the monomeric subunit) is 16.2 cal/K mol-residue [42], while for the dimeric ROP (63 residues in the monomer) ΔC_p=19.5 cal/K mol-residue [43]. Moreover, the per-mole-of-residue value for ΔH_{cal}=0.43 kcal/mol-residue is also considerably small for a protein of the size of BRCT-tan [44]. Such results indicate that thermally denatured BRCT-tan is likely to have undergone only partial unfolding. Additional unfolding may take place at higher temperatures where the second thermal anomaly also associated with aggregation and precipitation occurs. In the chemical denaturation studies an almost completely unstructured intermediate state has been demonstrated [22].

3.2. CD spectroscopy

CD spectroscopy of BRCT-tan reveals that the pH-induced dimerization bears negligible effects upon the structure of monomer BRCT-tan. The far-UV CD spectra at pH 7.0 and pH 9.0 are identical (Fig. 1). In addition, near-UV spectra present minute changes that can be associated to contributions from a small number of tyrosine and/or tryptophan side chains at the dimer interface.

In agreement to the DSC results, thermal CD scans at various wavelengths at pH 6.0, 7.0, and 9.0 show that BRCT-tan exhibits an irreversible denaturing transition at temperatures T_m ranging from 47 to 51 °C. For pH 6.0 and 7.0, the denatured state is prone to aggregation regardless of the salt content of the solution. Aggregation directly affects signal absorption, and the characterization of the denatured state is thus seriously impaired. A far more interesting situation arises in the case of dimer BRCT-tan at pH 9.0, 10 mM Tris–HCl. Heat denaturation occurs at T_m ~47.1 °C (Fig. 8A). In agreement with the DSC results, T_m increases with protein concentration indicating dissociation into monomers [38]. The denaturing reaction was found to be irreversible regardless of the final heating temperature and the total amount of time the system spent in the denatured state. The far- and near-UV CD spectra at any $T>T_m$, as well as those acquired at room temperature after cooling from the denatured state are all identical, confirming that no refolding occurs upon cooling below T_m.

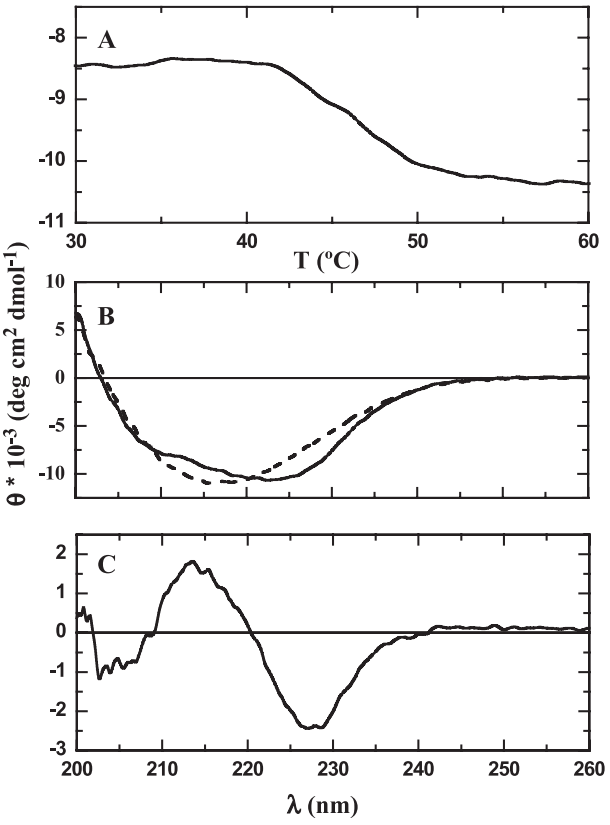

Fig. 8. (A) Characteristic thermal CD scan for dimer BRCT-tan at λ=213.5 nm (relatively large difference between native and denatured spectra), C_t=0.48 mg/ml, heating scan rate u=1.5 K/min. (B) Normalized far-UV CD spectra for dimer BRCT-tan at 25 °C (solid line) and at 58 °C (dashed line), ~10° higher than the heat denaturation transition temperature T_m. C. The difference (native–denatured) spectrum: the characteristic splitting centered at 225 nm may be attributed to small changes in the secondary structure and also to conformational changes in the environment of tryptophan side chains.

The far-UV CD spectra of native and denatured BRCT-tan are presented in Fig. 8B. Analysis of the denatured CD spectrum shows a reduction of less than 10% in the α-helical content and a corresponding increase of ~6% in β-structure with respect to the native. Such results are indicative of only small-scale restructuring in the denatured state. The far-UV difference spectrum (Fig. 8C) exhibits the characteristic features of a couplet, showing the symmetric splitting centered on 220 nm [45]. Besides limited changes in the secondary structure, local conformational changes in the environment of aromatic side chains may significantly contribute to difference-far-UV-CD-spectra similar to the one observed here [46,47]. Grishina and Woody [45] have theoretically predicted such difference-spectra by considering interactions of tryptophan, phenylalanine, and tyrosine side chains with neighboring ones. The specific negative couplet observed for dimer BRCT-tan bears great resemblance to the analogous spectrum for α-lactalbumin that has been attributed mainly to the 220–225 nm band (B_b) of the indole chromophore of tryptophan [48].

Normalized near-UV CD spectra above and below the thermal unfolding temperature are presented in Fig. 9. They exhibit very small differences demonstrating that the tertiary structure of denatured BRCT-tan maintains the overall characteristics of the native. These weak differences [best illustrated in the native-denatured difference spectrum (Fig. 9B)] are directly associated with the exposure of hydrophobic aromatic side chains to the solvent. A sharp low-intensity band at 295 nm is the most distinct feature, while a second lower-intensity band at ~260 nm is also detectable, although barely so. The band at 295 nm is primarily linked to tryptophan side chains (highest extinction coefficient), while the band at 260 nm is often attributed to phenylalanine [49]. The CD results reported here are certainly very different from the corresponding ones for the chemical denaturation of BRCT-tan; the reported far-UV CD spectra for the intermediate demonstrated a state that was not specifically structured, while the denatured state was totally unstructured [22].

The structure of BRCT-tan is illustrated in Fig. 10, depicting the locations of the molecule's five tryptophan residues. It can straightforwardly be observed that Trp1782 located at the hydrophobic inter-BRCT contact region (region A in Fig. 10) can be exposed to the solvent via a thermally induced disruption of the inter-BRCT interface. Analogously limited restructuring of the linker region, involving the disruption of the linker's interface with the BRCT repeats (region B in Fig. 10) can lead to the exposure

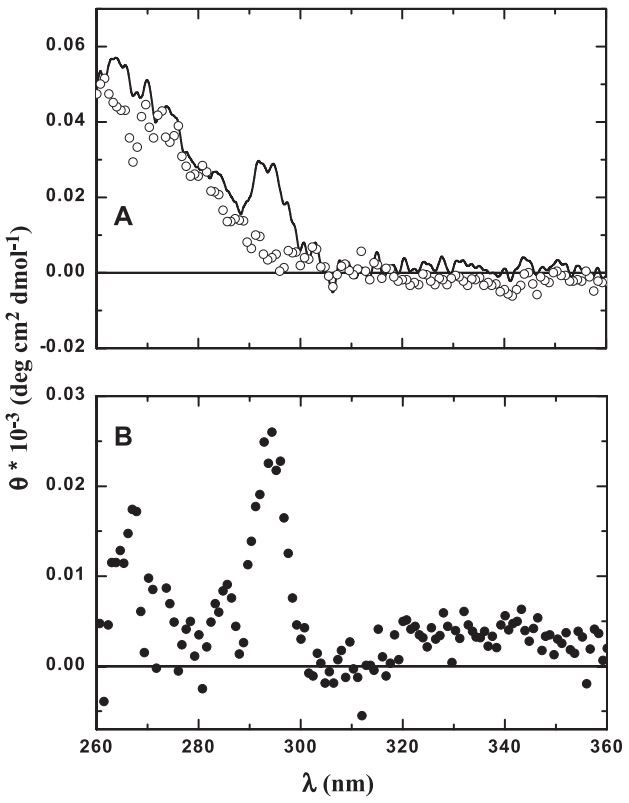

Fig. 9. (A) Normalized near-UV CD spectra for dimer BRCT-tan at 25 °C (solid line) and at 58 °C (open circles). The denatured state maintains most of the native's tertiary structure characteristics. (B) The difference (native–denatured) spectrum displays a sharp, positive band centered at 295 nm that can be associated with tryptophan residues becoming exposed to the solvent upon denaturation.

of Trp1712. On the other hand, major unfolding would be required to induce changes in the environment of Trp1718 or Trp1837. They are both buried in the hydrophobic core of the N-terminal and C-terminal BRCT repeats, respectively, and their exposure to the solvent would substantially affect the structural integrity of the molecule, in contrast to the DSC and CD results. For Trp1815, conclusive arguments cannot be presented. It is located at the flexible region (a.a. 1813–1821). Coordinates for its side chain could not be determined crystallographically [13]. Changes in the environment of aromatic side chains located at the linker region and the inter-BRCT-repeat interface, such as Tyr1703, Phe1704, and Tyr1845, are also expected to contribute to the obtained spectra. Minor contributions to the near-UV difference spectrum will arise from aromatic side chains along the dimeric interface.

3.3. Structure-based analysis

The application of structure-based analysis Eqs. (1a) (1b) (1c) and (2) for the denaturation of the entire BRCT-tan molecule, not surprisingly, leads to estimates of the thermodynamic parameters ΔC_p and ΔH_{cal} that are three to four times larger than the obtained experimental results. Based upon the structure of BRCT-tan [13], the individual contributions to ΔC_p and ΔH_{cal} can be estimated arising from the unfolding of specific regions of the molecule. Because all the spectroscopic evidence and the calorimetric results concur that the thermally denatured BRCT-tan is structurally very similar to the native, and the hydrophobic inter-BRCT-repeat pocket is crucial for the molecule's

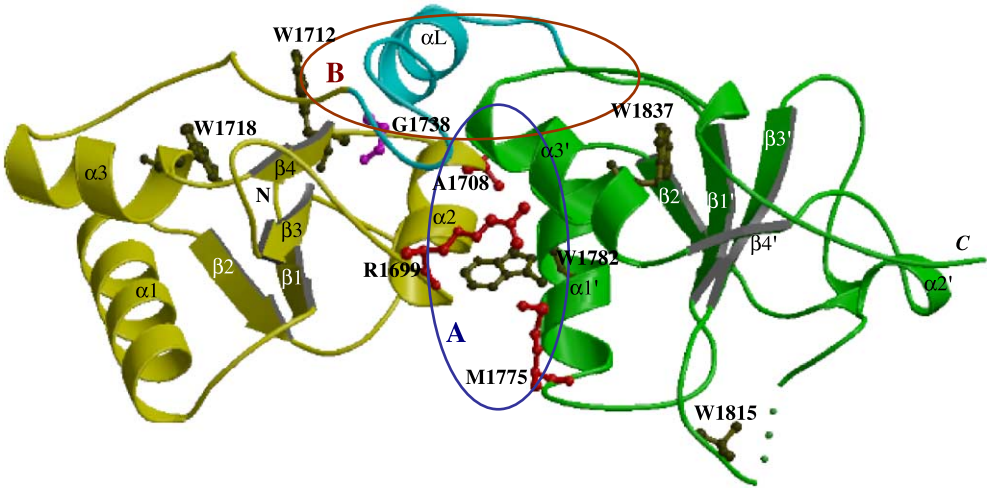

Fig. 10. Ribbon representation of human BRCT-tan structure adapted from Williams et al. [13] (RCSB entry: 1JNX). The N-terminal and C-terminal BRCT repeats are colored in yellow and green, respectively. The flexible interrepeat linker is colored in cyan. Secondary structure elements of the C-terminal BRCT repeat are labeled with 'prime'. Tryptophan residues shown here in order to facilitate the discussion of the CD results are depicted as dark-green balls-and-sticks. Residues, mutations of which have been linked to hereditary breast/ovarian cancer, are colored in red. Gly1738, mutations of which are discussed in the text, is colored in magenta. Green spheres depict a disordered region missing from the crystal structure. The ellipsoidal frames A and B mark the approximate boundaries of respective regions A (inter-BRCT-repeat interface) and B (linker-BRCT-repeats interface) considered in the structure-based analysis.

function, the structure-based analysis was focused upon (A) the disruption of the hydrophobic inter-BRCT-repeat contact surface (region A in Fig. 10) and (B) the disruption of the inter-BRCT-repeat-linker interface (region B in Fig. 10). Either (A) or (B) or both can take place without seriously affecting the overall structural integrity of the individual BRCT repeats. Finally, the disruption of (C), the BRCT-tan–BRCT-tan dimeric surface (for comparison with the experimental results at pH 9.0) must also be considered.

All the results are presented in Table 2. Applying Eqs. (1a) (1b) (1c) and (2) for the hydrophobic inter-BRCT-repeat interface (region A in Fig. 10) leads to ΔC_p=0.30 kcal/K mol and ΔH_{cal}=7.4 kcal/mol at T=47 °C. Analogous calculations concerning the linker and its interface with the two BRCT repeats (region B in Fig. 10) lead to ΔC_p=0.17 kcal/K mol and ΔH_{cal}=29.9 kcal/mol. The sum of the contributions from these two regions ΔC_p=0.47 kcal/K mol comes relatively close to the experimental result $(\Delta C_p)_{exp}$=0.60±0.08 kcal/K mol. On the other hand, ΔH_{cal}=37.3 kcal/mol is not comparable to the corresponding $(\Delta H_{cal})_{exp}$=92.6±5.6 kcal/mol. Because thermal unfolding involves the dissociation of the dimer, the observed differences must be attributed primarily to the disruption of the dimeric BRCT-tan interface (region C in Table 2). The small difference in ΔC_p is indicative of an equivalent change in the polar/apolar ASA upon the disruption of the dimeric interface, while the large difference in ΔH_{cal} points towards a sizeable enthalpic contribution form water molecules at the dimeric interface. The latter must also be responsible for the observed difference in the $(\Delta H_{cal})_{exp}$ values between monomeric and dimeric BRCT-tan.

The lack of a model for the structure of dimer BRCT-tan is an obstacle in the structure-based calculation. However, because the contribution from the dimeric surface to ΔC_p appears to be small and CD spectroscopy revealed only minute structural changes between monomer and dimer, we have proceeded by trying out a representative dimeric surface (Fig. 11) dictated by the packing in the crystal structure [13]. In the crystals of BRCT-tan, two symmetry-related molecules (crystallographic symmetry operation: -Y, -X, 5/6-Z) could form a putative dimer. The two monomers are related by a twofold symmetry in a head-to-head arrangement. The dimer interface is mainly constructed by the interaction of the α1 helices, which pack against each other in a parallel arrangement at a crossing angle of 44.5°. A second interface region exists involving the loop connecting α1′ and β1′ and its symmetric one, as well as the flexible region (a.a. 1813–1821). A total of 16 polar residues burying 364 Å^2 and 18 apolar residues burying 630 Å^2 constitute the dimer interface. Atoms from the flexible region, with missing coordinates, have not been included in these estimates. The dimeric interface (994 Å^2) amounts to 4.8% of the total ASA. This corresponds to less than 1% probability that the proposed dimer is formed by random monomer–monomer interactions (as other packing contacts in the crystal) [50], indicating a high degree of specificity.

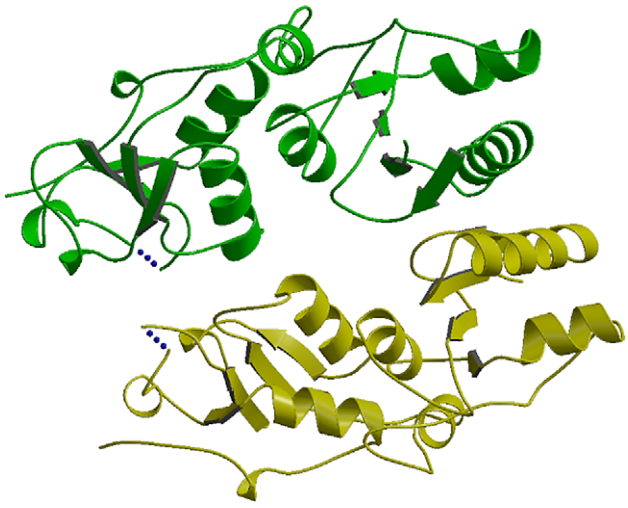

Fig. 11. Ribbon representation of a possible 3D structure of dimer BRCT-tan used for structure-based calculations (see text). The two monomers are colored in green and yellow, respectively. The dimeric surface is extracted directly from the crystal packing of BRCT-tan [13] as described in the text. Blue spheres correspond to the disordered region missing from the crystal structure.

Table 2
Structure-based estimates of ΔC_p and ΔH_{cal}

	# Apolar (a.a.)	ΔASA_{ap} (Å^2)	# Polar (a.a.)	ΔASA_{pol} (Å^2)	ΔC_p (kcal/K mol)	ΔH_{cal} (kcal/mol)
A. Disruption of the inter-BRCT-repeat interface (region A, Fig. 10)	16	764	9	248	0.30	7.4
B. Disruption of the linker interface with the two BRCT repeats (region B, Fig. 10)	22	747	21	813	0.17	29.9
C. Disruption of dimer BRCT-tan interface	9	315	8	182	0.11	6.2
D. Contribution from nine water molecules (per monomer) at the dimer interface	–	–	–	–	–	8.0–30.0
Total partial unfolding and dimer dissociation	47	1826	38	1243	0.58	51.5–73.5

Structure-based estimates of ΔC_p and ΔH_{cal} at T=47 °C for the thermal unfolding of selected regions A, B of BRCT-tan (see Fig. 10), and C the dimeric interface. The number of polar/apolar residues in each selected region is given along with the values for the change in the solvent accessible area (ΔASA), calculated by the DSSP program. The enthalpic contribution of water molecules at the dimeric interface is discussed in the text.

Applying Eqs. (1a) (1b) (1c) and (2) for the disruption of the dimeric interface leads to ΔC_p=0.11 kcal/K mol and ΔH_{cal}=6.2 kcal/mol at T=47 °C.

The total estimated ΔC_p, including contributions from regions (A), (B), and (C), is ΔC_p=0.58 kcal/K mol. This result is in excellent agreement with the DSC experiments. For the corresponding total estimate for ΔH_{cal}, in addition to the contribution from regions (A), (B), and (C), one must also consider the contribution from water molecules buried along the dimeric interface. Indeed, for the dimeric surface at hand, there exist at least 18 such water molecules (identified in the crystal structure of BRCT-tan [13]). A contribution to ΔH_{cal} of ~8 kcal/mol at 47 °C [30] is a possible lower bound. On the other hand, a corresponding upper bound, using data from crystalline salt hydrates, may be set to ~30 kcal/mol at 47 °C [51–53]. These values lead to a total estimated ΔH_{cal}=51.5 (lower bound) to 73.5 kcal/mol (upper bound), which is comparable to the experimental result $(\Delta H_{cal})_{exp}$=92.6±5.6 kcal/mol. Several reasons may have led to the underestimation of ΔH_{cal}: (A) in solution, a larger network of water molecules is expected to contribute to the enthalpy change than the 18 molecules considered at the dimeric surface, based on the crystal structure. (B) Additional unfolding occurring in other regions of BRCT-tan not necessarily affecting the value of ΔC_p (by exposing approximately equivalent polar–apolar surfaces). (C) A substantially different dimeric surface.

It has become apparent that structure-based calculations carried out under the hypothesis that the thermal unfolding of BRCT-tan involves the region around the BRCT–BRCT interface and the linker, led to estimates for ΔH_{cal} and especially for ΔC_p that are consistent with the DSC results. Of course, structure-based predictions are good indicators but they do not constitute proof for the underlying partial unfolding mechanism. However, it is notable that besides the overall good agreement with the calorimetric results, the proposed regional partial unfolding gains further support from the CD results, because all three Trp1712, Trp1782, Trp1815 or any combination of them may well become exposed to the solvent (Fig. 10).

4. Discussion

As evidenced by CD and high-precision DSC, thermally denatured BRCT-tan bears significant structural similarity to the native state. Structure-based analysis has shown consistency between theoretical estimates and experimental DSC results, when partial thermal unfolding is considered, contained within the region of the hydrophobic contact surface of the two BRCT repeats and the interrepeat linker. Partial thermal unfolding of this hydrophobic pocket is consistent with the results from CD spectroscopy. It is thus proposed that thermal denaturation to an intermediate fold is likely to involve disruptions within the inter-BRCT-repeat interface region induced by changes in the relative position of the two BRCTs. Such conformational changes may have only limited effects upon the structural integrity of the individual repeats, in agreement with the CD results. Moreover, they can be structurally accommodated because of the flexibility of the inter-BRCT linker. The thermally denatured state will have propensity to aggregate because up to 1500 Å^2 of hydrophobic surface per molecule may become accessible to the solvent. Further unfolding of the solidly packed BRCT repeats to a fully unstructured denatured state (such as the chemically denatured state [22]) will occur at higher temperatures, as indeed is evidenced by the DSC experiments, although the high-temperature DSC peak is severely affected by aggregation and precipitation.

Williams et al. [13] predicted a mutation-induced destabilization mechanism involving the disruption of the hydrophobic inter-BRCT-repeat interface for the cancer causing mutations M1775R, A1708E, and R1699W (Fig. 9). The likely existence of a thermal unfolding intermediate bearing structural and thermodynamic characteristics consistent with a possible inter-BRCT-repeat interface disruption provides substantial support to this prediction. Analogously, missense mutations located at the interrepeat linker, such as G1738E, for whom loss of function has been shown in vitro, [3] and G1738R, which has been detected in patients from nonrelated families with history of breast–ovarian cancer [54] may similarly destabilize the inter-BRCT interface.

The recent crystallographic [19–21] and NMR studies [55] of the complex of human BRCT-tan with phosphorylated peptides revealed the importance of the structural integrity of the conserved hydrophobic groove at the inter-BRCT-repeat interface for the molecule's ability to bind the pSe-*X*-*X*-Phe motif. Denaturation of BRCT-tan leading to a change in the relative position of the two repeats, as proposed here, will severely diminish the molecule's binding affinity due to the "two-knob" binding mechanism, requiring a specific distance between the phosphoserine binding site at the N-terminal BRCT repeat and the phenylalanine binding contact on the C-terminal repeat. Folding intermediates of BRCT-tan have been reported, although, contrary to the results presented here, they are not specifically structured. So far, besides the almost unstructured intermediate identified by chemical denaturation [22], a partly folded intermediate has also been reported for the tandem BRCT repeats in 53BP1 [56]. To our knowledge, this is the first report of a thermally induced partly unfolded denatured state of BRCT-tan showing evidence for the disruption of the inter-BRCT-repeat interface.

Acknowledgements

S.P. and A.L. acknowledge support from the Graduate Fellowship Program of NCSR "Demokritos". We would like to thank Prof. A. Monteiro for kindly providing the BRCT plasmids. The use of the facilities of the Centre for

Crystallographic Studies of Macromolecules of NCSR "Demokritos" is acknowledged. This work was supported by funding from the General Secretariat of Research and Technology of Greece.

References

[1] P.A. Futreal, Q. Liu, D. Shattuck-Eidens, C. Cochran, K. Harshman, S. Tavtigian, L.M. Bennett, A. Haugen-Strano, J. Swensen, Y. Miki, et al., BRCA1 mutations in primary breast and ovarian carcinomas, Science 266 (1994) 120–122.

[2] Y. Miki, J. Swensen, D. Shattuck-Eidens, P.A. Futreal, K. Harshman, S. Tavtigian, Q. Liu, C. Cochran, L.M. Bennett, W. Ding, et al., A strong candidate for the breast and ovarian cancer susceptibility gene BRCA1, Science 266 (1994) 66–71.

[3] F. Hayes, C. Cayanan, D. Barilla, A.N. Monteiro, Functional assay for BRCA1: mutagenesis of the COOH-terminal region reveals critical residues for transcription activation, Cancer Res. 60 (2000) 2411–2418.

[4] A.N. Monteiro, A. August, H. Hanafusa, Common BRCA1 variants and transcriptional activation, Am. J. Hum. Genet. 61 (1997) 761–762.

[5] J.S. Humphrey, A. Salim, M.R. Erdos, F.S. Collins, L.C. Brody, R.D. Klausner, Human BRCA1 inhibits growth in yeast: potential use in diagnostic testing, Proc. Natl. Acad. Sci. U. S. A. 94 (1997) 5820–5825.

[6] A.R. Venkitaraman, Cancer susceptibility and the functions of BRCA1 and BRCA2, Cell 108 (2002) 171–182.

[7] K.L. Nathanson, R. Wooster, B.L. Weber, K.N. Nathanson, Breast cancer genetics: what we know and what we need, Nat. Med. 7 (2001) 552–556.

[8] K. Yamane, M. Kawabata, T. Tsuruo, A DNA-topoisomerase-II-binding protein with eight repeating regions similar to DNA-repair enzymes and to a cell-cycle regulator, Eur. J. Biochem. 250 (1997) 794–799.

[9] T. Huyton, P.A. Bates, X. Zhang, M.J. Sternberg, P.S. Freemont, The BRCA1 C-terminal domain: structure and function, Mutat. Res. 460 (2000) 319–332.

[10] K. Yamane, T. Tsuruo, Conserved BRCT regions of TopBP1 and of the tumor suppressor BRCA1 bind strand breaks and termini of DNA, Oncogene 18 (1999) 5194–5203.

[11] X. Zhang, S. Morera, P.A. Bates, P.C. Whitehead, A.I. Coffer, K. Hainbucher, R.A. Nash, M.J. Sternberg, T. Lindahl, P.S. Freemont, Structure of an XRCC1 BRCT domain: a new protein–protein interaction module, EMBO J. 17 (1998) 6404–6411.

[12] V.V. Krishnan, K.H. Thornton, M.P. Thelen, M. Cosman, Solution structure and backbone dynamics of the human DNA ligase IIIalpha BRCT domain, Biochemistry 40 (2001) 13158–13166.

[13] R.S. Williams, R. Green, J.N. Glover, Crystal structure of the BRCT repeat region from the breast cancer-associated protein BRCA1, Nat. Struct. Biol. 8 (2001) 838–842.

[14] D.J. Derbyshire, B.P. Basu, L.C. Serpell, W.S. Joo, T. Date, K. Iwabuchi, A.J. Doherty, Crystal structure of human 53BP1 BRCT domains bound to p53 tumour suppressor, EMBO J. 21 (2002) 3863–3872.

[15] W.S. Joo, P.D. Jeffrey, S.B. Cantor, M.S. Finnin, D.M. Livingston, N.P. Pavletich, Structure of the 53BP1 BRCT region bound to p53 and its comparison to the Brca1 BRCT structure, Genes Dev. 16 (2002) 583–593.

[16] I.A. Manke, D.M. Lowery, A. Nguyen, M.B. Yaffe, BRCT repeats as phosphopeptide-binding modules involved in protein targeting, Science 302 (2003) 636–639.

[17] M. Rodriguez, X. Yu, J. Chen, Z. Songyang, Phosphopeptide binding specificities of BRCA1 COOH-terminal (BRCT) domains, J. Biol. Chem. 278 (2003) 52914–52918.

[18] X. Yu, C.C. Chini, M. He, G. Mer, J. Chen, The BRCT domain is a phospho-protein binding domain, Science 302 (2003) 639–642.

[19] R.S. Williams, M.S. Lee, D.D. Hau, J.N. Glover, Structural basis of phosphopeptide recognition by the BRCT domain of BRCA1, Nat. Struct. Mol. Biol. 11 (2004) 519–525.

[20] J.A. Clapperton, I.A. Manke, D.M. Lowery, T. Ho, L.F. Haire, M.B. Yaffe, S.J. Smerdon, Structure and mechanism of BRCA1 BRCT domain recognition of phosphorylated BACH1 with implications for cancer, Nat. Struct. Mol. Biol. 11 (2004) 512–518.

[21] E.N. Shiozaki, L. Gu, N. Yan, Y. Shi, Structure of the BRCT repeats of BRCA1 bound to a BACH1 phosphopeptide: implications for signaling, Mol. Cell 14 (2004) 405–412.

[22] C.M. Ekblad, H.R. Wilkinson, J.W. Schymkowitz, F. Rousseau, S.M. Freund, L.S. Itzhaki, Characterisation of the BRCT domains of the breast cancer susceptibility gene product BRCA1, J. Mol. Biol. 320 (2002) 431–442.

[23] Z. Wang, J. Moult, SNPs, protein structure, and disease, Human Mutat. 17 (2001) 263–270.

[24] S. Sunyaev, V. Ramensky, I. Koch, W. Lathe III, A.S. Kondrashov, P. Bork, Prediction of deleterious human alleles, Hum. Mol. Genet. 10 (2001) 591–597.

[25] S.C. Gill, P.H. Hipell, Calculation of protein extinction coefficients from amino acid sequence data, Anal. Biochem. 182 (1989) 319–326.

[26] U.K. Laemmli, Cleavage of structural proteins during the assembly of the head of bacteriophage T4, Nature 227 (1970) 680–685.

[27] V.V. Plotnikov, J.M. Brandts, L.N. Lin, J.F. Brandts, A new ultrasensitive scanning calorimeter, Anal. Biochem. 250 (1997) 237–244.

[28] K. Takahashi, J.M. Sturtevant, Thermal denaturation of streptomyces subtilisin inhibitor, subtilisin BPN', and the inhibitor–subtilisin complex, Biochemistry 20 (1981) 6185–6190.

[29] J. Gomez, V.J. Hilser, D. Xie, E. Freire, The heat capacity of proteins, Proteins 22 (1995) 404–412.

[30] V.J. Hilser, J. Gomez, E. Freire, The enthalpy change in protein folding and binding: refinement of parameters for structure-based calculations, Proteins 26 (1996) 123–133.

[31] W. Kabsch, C. Sander, Dictionary of protein secondary structure: pattern recognition of hydrogen-bonded and geometrical features, Biopolymers 22 (1983) 2577–2637.

[32] S.W. Provencher, J. Glockner, Estimation of globular protein secondary structure from circular dichroism, Biochemistry 20 (1981) 33–37.

[33] M.A. Andrade, P. Chacon, J.J. Merelo, F. Moran, Evaluation of secondary structure of proteins from UV circular dichroism spectra using an unsupervised learning neural network, Protein Eng. 6 (1993) 383–390.

[34] N. Sreerama, R.W. Woody, Protein secondary structure from circular dichroism spectroscopy. Combining variable selection principle and cluster analysis with neural network, ridge regression and self-consistent methods, J. Mol. Biol. 242 (1994) 497–507.

[35] G. Bohm, R. Muhr, R. Jaenicke, Quantitative analysis of protein far UV circular dichroism spectra by neural networks, Protein Eng. 5 (1992) 191–195.

[36] B. Dalmas, G.J. Hunter, W.H. Bannister, Prediction of protein secondary structure from circular dichroism spectra using artificial neural network techniques, Biochem. Mol. Biol. Int. 34 (1994) 17–26.

[37] J.M. Sanchez-Ruiz, Theoretical analysis of Lumry–Eyring models in differential scanning calorimetry, Biophys. J. 61 (1992) 921–935.

[38] J.M. Sturtevant, Biochemical application of differential scanning calorimetry, Annu. Rev. Phys. Chem. 38 (1987) 463–488.

[39] M. Thorolfsson, B. Ibarra-Molero, P. Fojan, S.B. Petersen, J.M. Sanchez-Ruiz, A. Martinez, L-phenylalanine binding and domain organization in human phenylalanine hydroxylase: a differential scanning calorimetry study, Biochemistry 41 (2002) 7573–7585.

[40] T. Vogl, C. Jatzke, H.J. Hinz, J. Benz, R. Huber, Thermodynamic stability of annexin V E17G: equilibrium parameters from an irreversible unfolding reaction, Biochemistry 36 (1997) 1657–1668.

[41] P.L. Privalov, S.A. Potekhin, Scanning microcalorimetry in studying temperature-induced changes in proteins, Methods Enzymol. 131 (1986) 4–51.
[42] M.J. Todd, N. Semo, E. Freire, The structural stability of the HIV-1 protease, J. Mol. Biol. 283 (1998) 475–488.
[43] M.W. Lassalle, H.J. Hinz, H. Wenzel, M. Vlassi, M. Kokkinidis, G. Cesareni, Dimer-to-tetramer transformation: loop excision dramatically alters structure and stability of the ROP four alpha-helix bundle protein, J. Mol. Biol. 279 (1998) 987–1000.
[44] C.G. Benitez-Cardoza, A. Rojo-Dominguez, A. Hernandez-Arana, Temperature-induced denaturation and renaturation of triosephosphate isomerase from *Saccharomyces cerevisiae*: evidence of dimerization coupled to refolding of the thermally unfolded protein, Biochemistry 40 (2001) 9049–9058.
[45] I.B. Grishina, R.W. Woody, Contributions of tryptophan side chains to the circular dichroism of globular proteins: exciton couplets and coupled oscillators, Faraday Discuss. (1994) 245–262.
[46] H.E. Auer, Far-ultraviolet absorption and circular dichroism spectra of L-tryprophan and some derivatives, J. Am. Chem. Soc. 95 (1973) 3003–3011.
[47] M.C. Manning, R.W. Woody, Theoretical study of the contribution of aromatic side chains to the circular dichroism of basic bovine pancreatic trypsin inhibitor, Biochemistry 28 (1989) 8609–8613.
[48] Z. Shi, R.W. Woody, N.R. Kallenbach, Is polyproline II a major backbone conformation in unfolded proteins? Adv. Protein Chem. 62 (2002) 163–240.
[49] R.W. Woody, Circular Dichroism and the Conformational Analysis of Biomolecules, Plenum Press, New York, 1996.
[50] J. Janin, Specific versus non-specific contacts in protein crystals, Nat. Struct. Biol. 4 (1997) 973–974.
[51] J.E. Ladbury, Just add water! The effect of water on the specificity of protein–ligand binding sites and its potential application to drug design, Chem. Biol. 3 (1996) 973–980.
[52] J.D. Dunitz, Win some, lose some: enthalpy–entropy compensation in weak intermolecular interactions, Chem. Biol. 2 (1995) 709–712.
[53] J. Dunitz, The entropic cost of bound water in crystals and biomolecules, Science 264 (1994) 670.
[54] A. Ladopoulou, C. Kroupis, I. Konstantopoulou, L. Ioannidou-Mouzaka, A.C. Schofield, A. Pantazidis, S. Armaou, I. Tsiagas, E. Lianidou, E. Efstathiou, C. Tsionou, C. Panopoulos, M. Mihalatos, G. Nasioulas, D. Skarlos, N.E. Haites, G. Fountzilas, N. Pandis, D. Yannoukakos, Germ line BRCA1 and BRCA2 mutations in Greek breast/ovarian cancer families: 5382insC is the most frequent mutation observed, Cancer Lett. 185 (2002) 61–70.
[55] M.V. Botuyan, Y. Nomine, X. Yu, N. Juranic, S. Macura, J. Chen, G. Mer, Structural basis of BACH1 phosphopeptide recognition by BRCA1 tandem BRCT domains, Structure (Camb). 12 (2004) 1137–1146.
[56] C.M. Ekblad, A. Friedler, D. Veprintsev, R.L. Weinberg, L.S. Itzhaki, Comparison of BRCT domains of BRCA1 and 53BP1: a biophysical analysis, Protein Sci. 13 (2004) 617–625.